Low-Temperature Solution Synthesis of Nanocrystalline Binary Intermetallic Compounds Using the Polyol Process

Robert E. Cable and Raymond E. Schaak*

Department of Chemistry, Texas A&M University, P.O. Box 30012, College Station, Texas 77842-3012

Received September 6, 2005. Revised Manuscript Received October 20, 2005

Nanocrystalline intermetallic powders have been synthesized from metal salt precursors at low temperatures using a modified polyol process with tetraethylene glycol as the solvent. This solution route has yielded several phase-pure compounds in the M−Sn (M = Ag, Au, Co, Cu, Fe, Ni), Pt−M′ (M′ = Bi, Pb, Sb, Sn), and Co−Sb bimetallic systems. In the Co−Sb system, CoSb and $CoSb_3$ can be selectively produced by controlling the initial metal concentrations and the reaction temperature. The Co−Sn and Cu−Sn systems can selectively form Co_3Sn_2 vs CoSn and Cu_6Sn_5 vs $Cu_{41}Sn_{11}$ during a single reaction as a function of temperature. These results demonstrate kinetic control over crystal structure in these intermetallic systems. The reaction progress may be monitored at different times and temperatures by XRD, giving insight into the reaction pathways. TEM micrographs show that the particle sizes in the M−Sn systems range from 5 to 50 nm, while the Pt−M′ systems range from 10 to 100 nm. SEM micrographs show that these particles aggregate to form densely packed 100−200 nm clusters. DSC data show that the intermetallics synthesized using the polyol process exhibit order−disorder phase transitions at temperatures near those expected for bulk powders. The nanocrystalline powders are redispersible in solution, and preliminary experiments have shown that they may be templated by nanoscale molds, allowing for solution-based materials processing applications.

Introduction

Intermetallic compounds are important functional materials that find use in a wide range of applications.[1] As atomically ordered compounds that span a range of compositions and crystal structures, intermetallics often exhibit physical properties that are superior to their atomically disordered alloy analogues. For example, intermetallic FePt is a room-temperature ferromagnet with high coercivity and magnetoanisotropy, which makes it promising for magnetic storage applications.[2] Likewise, PtBi exhibits enhanced electrocatalytic activity compared to Pt and is virtually immune to CO poisoning.[3] Important properties of other transition-metal intermetallics include superconductivity,[4] shape memory effects,[5] magnetoresistance,[6] high structural strength at elevated temperatures,[7] and solid-state hydrogen storage capability.[8]

Bulk powders of intermetallic compounds are traditionally synthesized using high-temperature arc melting or powder metallurgy techniques, which often require several days of annealing to obtain the desired structures. While highly successful for synthesizing many important intermetallics, this traditional method does have some limitations. First, the final products are generally those that are thermodynamically stable. Thus, it is difficult to access metastable phases or structures that are only stable at low temperatures. Second, reaction pathways are usually unknown, precluding kinetic control over phase formation. Third, it can be very difficult to control the crystallite size and morphology using high-temperature methods, which favor grain growth and the formation of large micrometer-scale crystallites.

Solution-based synthetic strategies offer several important advantages over traditional high-temperature methods.[9] For example, solution routes can precipitate nanocrystalline powders at low temperatures where bulk-phase solid-state reaction kinetics are typically too slow to facilitate reactivity.[10] Also, solution methods often allow control over nanostructure and morphology, providing a convenient medium for growing size- and shape-controlled nanocrys-

* To whom correspondence should be addressed. E-mail: schaak@mail.chem.tamu.edu. Phone: (979) 458-2858. Fax: (979) 845-4719.

(1) (a) Sauthoff, G. *Intermetallics*; Wiley: New York, 1995. (b) Cahn, R. W. *Contemp. Phys.* **2001**, *42*, 365−375.
(2) (a) Sun, S.; Murray, C. B.; Weller, D.; Folks, L.; Moser, A. *Science* **2000**, *287*, 1989−1992. (b) Sun, S.; Anders, S.; Thomson, T.; Baglin, J. E. E.; Toney, M. F.; Hamann, H. F.; Murray, C. B.; Terris, B. D. *J. Phys. Chem. B* **2003**, *107*, 5419−5425.
(3) (a) Casado-Rivera, E.; Gal, Z.; Angelo, A. C. D.; Lind, C.; DiSalvo, F. J.; Abruna, H. D. *Chem. Phys. Chem.* **2003**, *4*, 193−199. (b) Casado-Rivera, E.; Volpe, D. J.; Alden, L.; Lind, C.; Downie, C.; Vazquez-Alvarez, T.; Angelo, A. C. D.; DiSalvo, F. J.; Abruna, H. D. *J. Am. Chem. Soc.* **2004**, *126*, 4043−4049. (c) Oana, M.; Hoffmann, R.; Abruna, H. D.; DiSalvo, F. J. *Surf. Sci.* **2005**, *574*, 1−16.
(4) (a) Cava, R. J.; Takagi, H.; Batlogg, B.; Zandbergen, H. W.; Krajewski, J. J.; Peck, W. F.; Vandover, R. B.; Felder, R. J.; Siegrist, T.; Mizuhashi, K.; Lee, J. O.; Eisaki, H.; Carter, S. A.; Uchida, S. *Nature* **1994**, *367*, 146−148. (b) He, T.; Huang, Q.; Ramirez, A. P.; Wang, Y.; Regan, K. A.; Rogado, N.; Hayward, M. A.; Haas, M. K.; Slusky, J. S.; Inumara, K.; Zandbergen, H. W.; Ong, N. P.; Cava, R. J. *Nature* **2001**, *411*, 54−56.
(5) Ullakko, K.; Huang, J. K.; Kantner, C.; O'Handley, R. C.; Kokorin, V. V. *Appl. Phys. Lett.* **1996**, *69*, 1966−1968.
(6) Van Dover, R. B.; Gyorgy, E. M.; Cava, R. J.; Krajewski, J. J.; Felder, R. J.; Peck, W. F. *Phys. Rev. B* **1993**, *47*, 6134−6137.
(7) Liu, C. T. *Mater. Chem. Phys.* **1995**, *42*, 77−86.
(8) (a) Kirchheim, R.; Mutschele, T.; Keininger, W.; Gleiter, H.; Birringer, R.; Koble, T. D. *Mater. Sci. Eng.* **1988**, *99*, 457−462. (b) Kamakoti, P.; Sholl, D. S. *J. Membr. Sci.* **2003**, *225*, 145−154.
(9) Stein, A.; Keller, S. W.; Mallouk, T. E. *Science* **1993**, *259*, 1558−1564.
(10) Leonard, B. M.; Bhuvanesh, N. S. P.; Schaak, R. E. *J. Am. Chem. Soc.* **2005**, *127*, 7326−7327.

10.1021/cm0520113 CCC: $30.25
Published on Web 11/19/2005

tals[11] and processing them into thin films[12] and nanotemplated materials.[13] Despite significant research effort aimed at developing solution-based routes to oxide and chalcogenide materials,[14] much less progress has been made in accessing reduced multi-metal compounds as nanocrystalline powders. A few nanocrystalline intermetallics have been accessed, but they typically require ball milling,[15] thermolysis,[16] chemical vapor deposition,[17] gas-phase condensation,[18] or high-temperature/high-pressure processing[19] to form. Intermetallics in general have been overlooked as synthetic targets of solution-based synthetic strategies. This is a significant shortcoming because the availability of general low-temperature solution routes for synthesizing nanocrystalline intermetallic compounds would likely open the door to many new and metastable phases as well as increased utilization in emerging nanotechnological applications.

The polyol process, which exploits high-boiling polyalcohol solvents that also act as mild reducing agents when heated, was originally developed for the synthesis of nanocrystalline powders of Pd and other late transition elements.[20−22] Since then, it has been modified to produce size- and shape-controlled nanocrystals of a variety of elements and alloys[11,23−26] and has yielded important magnetic, catalytic, and optical nanomaterials. Recently, we reported that intermetallic nanocrystals and nanocrystalline powders could be synthesized using low-temperature solution routes, including a modified polyol process.[10,13,27,28] This approach bypasses the high-temperature melting step that is often required in traditional bulk syntheses of intermetallics and greatly reduces the time required to form them. Importantly, we have also shown that new ternary intermetallic compounds having structures not observed using traditional bulk syntheses can be stabilized as nanocrystals using the polyol process.[10]

Here, we show that the polyol process is general for the rapid low-temperature synthesis of nanocrystalline intermetallics, successfully yielding phase-pure binary intermetallics in the M−Sn (M = Ag, Au, Co, Cu, Fe, Ni), Pt−M′ (M′ = Bi, Pb, Sb, Sn), and Co−Sb systems. These systems were chosen because (a) the Sn-based systems show a variety of interesting magnetic, electronic, and electrochemical properties,[29−34] (b) the Pt-based systems are of interest for their catalytic properties,[3] and (c) the Co−Sb system has well-known size-dependent thermoelectric properties.[35−37] In addition to the known phases that can be formed, these results have important implications for possibly synthesizing new and metastable intermetallics using low-temperature solution methods. Also, since a variety of modifications to the polyol process are known to yield well-formed monodisperse nanocrystals,[2,11] it is reasonable to anticipate similar morphological control for intermetallic systems. This would impact fields such as magnetic information storage, nanoscale electronics, self-assembled nanocomposites, and catalysis, for which the limited number of existing intermetallic nanocrystals are known to yield superior properties.

Experimental Section

Materials. The following metal reagents were used: $SnCl_2$ (anhydrous, 99% min.), $Sn[CH_3(CH_2)_3CH(C_2H_5)CO_2]_2$, $Cu(C_2H_3O_2)_2 \cdot H_2O$ (98.0−102.0%), $HAuCl_4 \cdot 3H_2O$ (99.99%), $AgNO_3$ (99.9+%),

(11) Wiley, B.; Sun, Y.; Mayers, B.; Xia, Y. *Chem. Eur. J.* **2005**, *11*, 454−463.

(12) (a) Kurihara, L. K.; Chow, G. M.; Schoen, P. E. *Nanostruct. Mater.* **1995**, *5*, 607−613. (b) Chow, G. M.; Kurihara, L. K.; Kemner, K. M.; Schoen, P. E.; Elam, W. T.; Ervin, A.; Keller, S.; Zhang, Y. D.; Budnick, J.; Ambrose, T. *J. Mater. Res.* **1995**, *10*, 1546−1554. (c) Yin, H.; Chow, G. M. *J. Mater. Res.* **2003**, *18*, 180−187.

(13) Schaak, R. E.; Sra, A. K.; Leonard, B. M.; Cable, R. E.; Bauer, J. C.; Han, Y.-F.; Means, J.; Teizer, W.; Vasquez, Y.; Funck, E. S. *J. Am. Chem. Soc.* **2005**, *127*, 3506−3515.

(14) (a) Wright, J. D.; Sommerdijk, A. J. M. *Sol−gel materials: chemistry and applications*; Gordon and Breach: Amsterdam, 2001. (b) Mitzi, D. B.; Kosbar, L. L.; Murray, C. E.; Copel, M.; Afzali, A. *Nature* **2004**, *428*, 299−303.

(15) (a) Koch, C. C.; Whittenberger, J. D. *Intermetallics* **1996**, *4*, 339−355. (b) Bai-Lin, Yu.; Xin-Feng, T.; Qiong, Q.; Qing-Jie, Z. *Acta Phys. Sin.* **2004**, *53*, 3130−3135. (c) Xie, J.; Zhao, X. B.; Cao, G. S.; Zhao, M. J.; Su, S. F. *J. Power Sources* **2005**, *140*, 350−354.

(16) (a) Rehbein, M.; Epple, M.; Fischer, R. D. *Solid State Sci.* **2000**, *2*, 473−488. (b) Heibel, M.; Kumar, G.; Wyse, C.; Bukovec, P.; Bocarsly, A. B. *Chem. Mater.* **1996**, *8*, 1504−1511. (c) Vondrova, M.; Majsztrik, P. W.; Gould, S.; Bocarsly, A. B. *Chem. Mater.* **2005**, *17*, 4755−4757.

(17) (a) Onda, A.; Komatsu, T.; Yashima, T. *J. Catal.* **2001**, *201*, 13−21. (b) Komatsu, T.; Inaba, K.; Uezono, T.; Onda, A.; Yashima, T. *Appl. Catal. A* **2003**, *251*, 315−326. (c) Onda, A.; Komatsu, T.; Yashima, T. *J. Catal.* **2003**, *221*, 378−385.

(18) Haubold, T.; Bohn, R.; Birringer, R.; Gleiter, H. *Mater. Sci. Eng.* **1992**, *A153*, 679−683.

(19) (a) Withers, J. C.; Shiao, H. C.; Loutfy, R. O.; Wang, P. *J. Miner. Met. Mater. Soc.* **1991**, *43*, 36−39. (b) Abe, O.; Tsuge, A. *J. Mater. Res.* **1991**, *6*, 928−934. (c) Haber, J. A.; Gunda, N. V.; Balbach, J. J.; Conradi, M. S.; Buhro, W. E. *Chem. Mater.* **2000**, *20*, 973−982. (d) Bonnemann, H.; Brijoux, W.; Hofstadt, H.-W.; Ould-Ely, T.; Schmidt, W.; Wassmuth, B.; Weidenthaler, C. *Angew. Chem., Int. Ed.* **2002**, *41*, 599−603.

(20) (a) Murray, C. B.; Kagan, C. R.; Bawendi, M. G. *Annu. Rev. Mater. Sci.* **2000**, *30*, 545−610. (b) Murray, C. B.; Sun, S.; Gaschler, W.; Doyle, H.; Betley, T. A.; Kagan, C. R. *IBM J. Res. Dev.* **2001**, *45*, 47−56.

(21) (a) Fievet, F.; Lagier, J. P.; Blin, B.; Beaudoin, B.; Figlarz, M. *Solid State Ionics* **1989**, *32/33*, 198−205. (b) Ducamp-Sanguesa, C.; Herrera-Urbina, R.; Figlarz, M. *Solid State Ionics* **1993**, *63−65*, 25−30.

(22) (a) Toshima, N.; Kushihashi, K.; Yonezawa, T.; Hirai, H. *Chem. Lett.* **1989**, *10*, 1769−1772. (b) Toshima, N.; Harada, M.; Yamazaki, Y.; Asakura, K. *J. Phys. Chem.* **1992**, *96*, 9927−9933. (c) Toshima, N.; Yonezawa, T. *New J. Chem.* **1998**, 1179−1201.

(23) (a) Sun, Y.; Mayers, B.; Herricks, T.; Xia, Y. *Nano Lett.* **2003**, *3*, 955−960. (b) Sun, Y.; Wiley, B.; Li, Z.-Y.; Xia, Y. *J. Am. Chem. Soc.* **2004**, *126*, 9399−9406.

(24) Hoefelmeyer, J. D.; Niesz, K.; Somorjai, G.; Tilley, T. D. *Nano Lett.* **2005**, *5*, 435−438.

(25) Kim, F.; Connor, S.; Song, H.; Kuykendall, T.; Yang, P. *Angew. Chem., Int. Ed.* **2004**, *43*, 3673−3677.

(26) Teng, X.; Yang, H. *Nano Lett.* **2005**, *5*, 885−891.

(27) Sra, A. K.; Schaak, R. E. *J. Am. Chem. Soc.* **2004**, *126*, 6667−6672.

(28) Sra, A. K.; Ewers, T. D.; Schaak, R. E. *Chem. Mater.* **2005**, *17*, 758−766.

(29) Hamilton, D. C.; Raub, C. J.; Matthias, B. T.; Corenzwit, E.; Hull, G. W. *J. Phys. Chem. Solids* **1965**, *26*, 665−667.

(30) Kuncser, V.; Doi, M.; Sahoo, B.; Stromberg, F.; Keune, W. *J. Appl. Phys.* **2003**, *94*, 3573−3581.

(31) Amadei, I.; Panero, S.; Scrosati, B.; Cocco, G.; Schiffini, L. *J. Power Sources* **2005**, *143*, 227−230.

(32) Massalski, T. B., Ed. *Binary Alloy Phase Diagrams*; ASM International: Materials Park, OH, 1996.

(33) Song, S. Q.; Zhou, W. J.; Zhou, Z. H.; Jiang, L. H.; Sun, G. Q.; Xin, Q.; Leontidis, V.; Kontou, S., Tsiakaras, P. *Int. J. Hydrogen Energy* **2005**, *30*, 995−1001.

(34) Hauser, J. J.; Theuerer, H. C.; Werthamer, N. R. *Phys. Rev.* **1964**, *136*, A637−A641.

(35) (a) Morelli, D. T.; Caillat, T.; Fleurial, J.-P.; Borshchevsky, A.; Vandersande, J.; Chen, B.; Uher, C. *Phys. Rev. B* **1995**, *51*, 9622−9628. (b) Sharp, J. W.; Jones, E. C.; Williams, R. K.; Martin, P. M.; Sales, B. C. *J. Appl. Phys.* **1995**, *78*, 1013−1018.

(36) (a) Toprak, M. S.; Stiewe, C.; Platzek, D.; Williams, S.; Bertini, L.; Müller, E.; Gatti, C.; Zhang, Y.; Rowe, M.; Muhammed, M. *Adv. Funct. Mater.* **2004**, *14*, 1189−1196.

(37) (a) Bai-Lin, Yu.; Xin-Feng, T.; Qiong, Q.; Qing-Jie, Z. *Acta Phys. Sin.* **2004**, *53*, 3130−3135. (b) Xie, J.; Zhao, X. B.; Cao, G. S.; Zhao, M. J.; Su, S. F. *J. Power Sources* **2005**, *140*, 350−354.

Table 1. Details for the Synthesis of Nanocrystalline M−Sn, Pt−M′, and Co−Sb Intermetallic Powders

intermetallic species	reagents	reaction molarity in M or M′ (mM)	M:M′ reaction ratio[a]	intermetallic phase formation temperature (°C)
Ag_4Sn	$AgNO_3$, tin(II) 2-ethylhexanoate	4.4 mM in Ag	1.0:1.0	175 °C
Au_5Sn	$HAuCl_4 \cdot 3H_2O$, tin(II) 2-ethylhexanoate	4.2 mM in Au	1.0:1.0	175 °C
Co_3Sn_2, CoSn	$Co(OOCCH_3)_2 \cdot 4H_2O$, $SnCl_2$	4.3 mM in Co	1.0:4.0	200 °C, 260 °C
Cu_6Sn_5, $Cu_{41}Sn_{11}$	$Cu(OOCCH_3)_2 \cdot H_2O$, $SnCl_2$	4.3 mM in Cu	1.0:5.0	125 °C, 275 °C
$FeSn_2$	$Fe(acac)_3$, $SnCl_2$	4.4 mM in Fe	1.0:5.9	125 °C
Ni_3Sn_4	$Ni(OOCCH_3) \cdot xH_2O$, $SnCl_2$	5.2 mM in Ni	1.0:4.4	190 °C
PtBi	$Bi(NO_3)_3 \cdot 5H_2O$, K_2PtCl_6	4.0 mM in Bi	1.0:1.0	220 °C
PtPb	$Pb(OOCCH_3)_2 \cdot 3H_2O$, K_2PtCl_6	4.5 mM in Pb	1.0:1.1	150 °C
PtSb	$SbCl_3$, K_2PtCl_6	4.7 mM in Sb	1.0:1.0	200 °C
PtSn	$SnCl_2$, K_2PtCl_6	23.0 mM in Sn	1.0:4.3	230 °C
CoSb	$Co(OOCCH_3)_2 \cdot 4H_2O$	5.7 mM in Co	1.0:3.0	175 °C
$CoSb_3$	$SbCl_3$	4.6 mM in Co	1.0:4.5	240 °C

[a] For M:Sn phases, M = (Ag, Au, Co, Cu, Fe, Ni) and M′ = Sn; for Pt−M phases, M = Pt and M′ = (Bi, Pb, Sb, Sn); for Co−Sb phases, M = Co and M′ = Sb.

K_2PtCl_6 (40.11% Pt), $Ni(C_2H_3O_2) \cdot xH_2O$ (99+%), $SbCl_3$ (99.9%), $Co(C_2H_3O_2)_2 \cdot 4H_2O$ (98.0−102.0%), $Fe(acac)_3$, $Pb(C_2H_3O_2)_2 \cdot 3H_2O$ (99.0−103.0%), and $Bi(NO_3)_3 \cdot 5H_2O$ (Mallinckrodt Chemical Works). The reducing agent, surface stabilizer, and solvent were $NaBH_4$ (98%), poly(vinyl pyrrolidone) (PVP, MW = 40000), and tetraethylene glycol (TEG, 99+%), respectively. All chemicals were purchased from Alfa Aesar unless otherwise noted.

Synthesis. The nanocrystalline intermetallic powders were synthesized by a modified polyol process, which has been previously reported.[10,28] For the M−Sn and Pt−M′ systems, the metal reagent was dissolved in 20 mL of TEG by sonication and magnetic stirring. $SnCl_2$, $Sn[CH_3(CH_2)_3CH(C_2H_5)CO_2]_2$ (for M−Sn) or K_2PtCl_6 (for Pt−M′), and PVP (170 mg) were then sequentially dissolved by the same means (see Table 1 for details). After the solution was vigorously stirred at room temperature under bubbling Ar for at least 45 min, 25 mg of $NaBH_4$ freshly dissolved in 5 mL of TEG was added slowly. Upon reduction, the solution usually turns a dark brown or black color and is then heated to the desired temperature (see Table 1). During the course of the reaction, 1.0 mL aliquots of the heated solution were collected to determine the appropriate reaction temperatures for intermetallic phase formation. Powders were precipitated from solution by centrifugation and were washed thoroughly with ethanol.

Characterization. Powder X-ray diffraction (XRD) data were collected on a Bruker GADDS three-circle X-ray diffractometer using Cu Kα radiation. Transmission electron microscopy (TEM) images, selected area electron diffraction (SAED) patterns, and energy-dispersive X-ray analysis (EDS) were collected using a JEOL JEM-2010 TEM. Samples were prepared by sonicating the nanocrystalline intermetallic powders in ethanol and dropping a small volume onto a carbon-coated nickel grid. Scanning electron microscopy (SEM) images were acquired using a JEOL JSM-6400 SEM. X-ray photoelectron spectroscopy (XPS) data were collected on a Kratos Ultra Axis Hsi 165 XPS using an Al anode set at 15 mA and 15 kV. Samples were prepared by sonicating the powder in ethanol and drop-coating a small volume onto a clean Si wafer. Differential scanning calorimetry (DSC) data were collected on a TA Instruments Q600 SDT under Ar. CHN analysis was performed by Atlantic Microlabs (Norcross, GA).

Results and Discussion

Synthesis of Nanocrystalline Binary Intermetallic Powders. TEG was used as a high-boiling solvent (T_{BP} = 310 °C) to allow for the one-pot solution synthesis of nanocrystalline binary intermetallic compounds.[28] The intermetallics are synthesized by dissolving the reagents in TEG, reducing them at room temperature with $NaBH_4$, and heating them to various temperatures between 100 and 300 °C. Aliquots taken at regular intervals provide information about phase formation, and often several distinct phases are observed during the reaction, depending on the temperature and time. The products formed upon reduction and prior to heating are generally multiphase, and the intermetallic phases are usually formed by 200 °C. The reaction times are typically very short, often requiring only the amount of time necessary to reach the final reaction temperature. The final products tend to contain 2−5 wt % of polymer residue, as determined by CHN analysis of several samples.

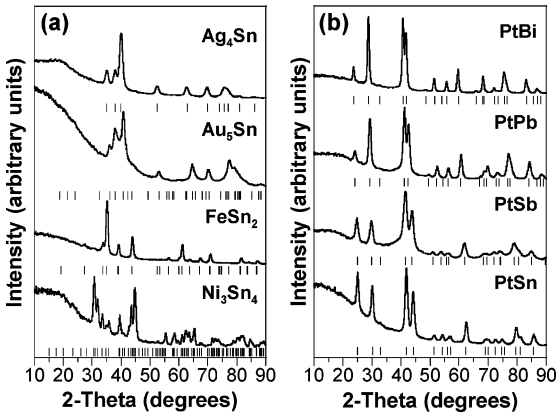

Figure 1. Powder XRD patterns for nanocrystalline intermetallics (a) M−Sn [Ag_4Sn, Au_5Sn, $FeSn_2$, Ni_3Sn_4] and (b) Pt−M′ [PtBi, PtPb, PtSb, PtSn]. Tick marks below each pattern represent allowed reflections for each compound.

To demonstrate the breadth of this synthetic technique for accessing nanocrystalline binary intermetallics, we chose to focus on the M−Sn (M = Ag, Au, Co, Cu, Fe, Ni), Pt−M′ (M′ = Bi, Pb, Sb, Sn), and Co−Sb systems. Table 1 presents a summary of the reagents and temperatures necessary to form phase-pure intermetallics in these systems, and Figure 1 shows representative XRD data for the intermetallic products. XRD data for selected M−Sn phases are shown in Figure 1a. All of these compounds are pure phases, within the detection limits of our laboratory diffractometer, and agree well with simulated XRD patterns based on prior literature reports. Au_5Sn, a known superconductor with T_c = 2 K,[29] and Ag_4Sn can be stabilized at 175 °C. These alloys crystallize in the Mg structure type (hcp), which Ag, Au,

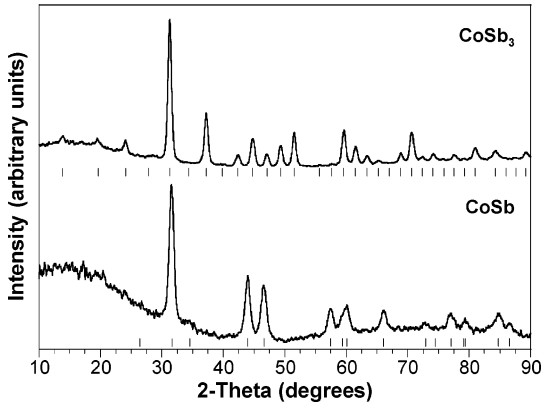

Figure 2. Powder XRD patterns for (top) $CoSb_3$ and (bottom) CoSb. Tick marks below each pattern represent allowed reflections for each compound.

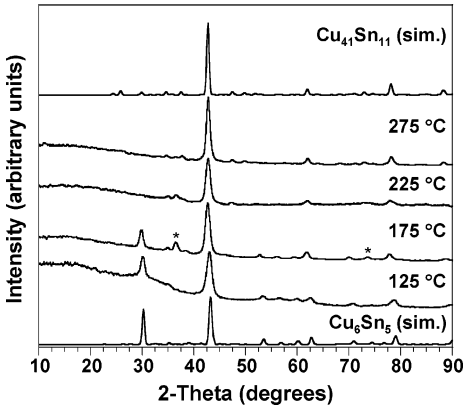

Figure 3. Powder XRD patterns for the products isolated as a function of heating temperature in the Cu−Sn system, along with simulated patterns (based on literature references) for (bottom) Cu_6Sn_5 and (top) $Cu_{41}Sn_{11}$. At 125 °C, the pattern matches that of Cu_6Sn_5. Upon further heating in the presence of tin, the pattern transforms to that expected for $Cu_{41}Sn_{11}$, indicating additional tin incorporation in the crystalline product. (The peaks near 36.5 and 73.7° 2θ in the intermediate-temperature samples, labeled with an asterisk (*), correspond to a Cu_2O impurity, which results from nanocrystalline Cu that has oxidized during sample handling under ambient conditions.)

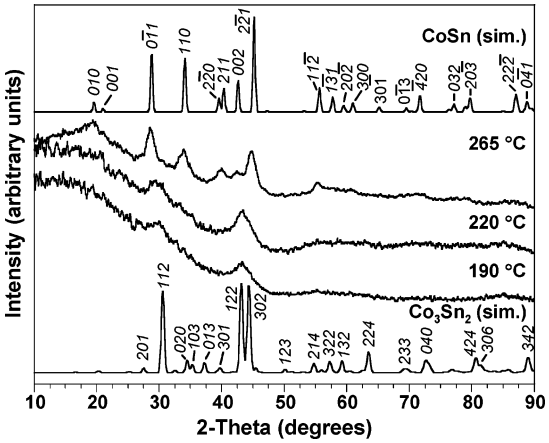

Figure 4. Powder XRD patterns for the products isolated as a function of heating temperature in the Co−Sn system, along with simulated patterns (based on literature references) for (bottom) Co_3Sn_2 and (top) CoSn. Between 190 and 200 °C, the pattern matches closely with that expected for Co_3Sn_2. Upon further heating in the presence of tin, the pattern transforms to that expected for CoSn, indicating additional tin incorporation in the crystalline product.

and Sn do not adopt. Al_2Cu-type $FeSn_2$, which is an antiferromagnet with a known thickness dependence of T_N in thin films,[30] forms as a pure phase upon heating for 30 min at 130 °C. Monoclinic Ni_3Sn_4 forms at 195 °C, which is significant because of the potential for using nanocrystalline Ni_3Sn_4 as an anode material in Li-ion batteries.[31] Nanocrystalline Ni_3Sn_4 has been produced by ball milling for up to 30 h,[31] and a direct solution route to a similar material may prove useful for battery applications.

Similarly, Pt−M′ intermetallics can also be synthesized using this rapid low-temperature solution approach (Figure 1b). As expected based on their respective binary phase diagrams, PtBi, PtPb, PtSb, and PtSn adopt the NiAs structure type.[32] PtBi and PtSn, of interest for their catalytic properties,[3,33] form phase-pure intermetallics near 250 °C. PtPb is known to be a superconductor with $T_c = 7.2$ K in layered thin films,[34] and we were able to access this phase at 165 °C. PtSb can be stabilized by 200 °C. In addition to the M−Sn and Pt−M′ systems, other binary intermetallic systems can be accessed. For example, CoSb and $CoSb_3$ can both be accessed in the Co−Sb system (Figure 2). $CoSb_3$ is a well-known thermoelectric prototype,[35] and reports have shown enhanced thermoelectric properties as the particle size decreases.[36] Methods for making nanocrystalline $CoSb_3$, however, typically require ball milling or solvothermal reactions with reaction times of 72 h.[37]

The Co−Sb system (Figure 2) demonstrates that multiple phase-pure intermetallics can be accessed in the same system. However, in some cases, two distinct intermetallic compounds can be synthesized in a single reaction with a fixed nominal composition. For example, in the Cu−Sn system (Figure 3), a 1:5 ratio of Cu:Sn yields NiAs-type Cu_5Sn_6 at 125 °C and $Cu_{41}Sn_{11}$ at 275 °C. As the solvent temperature increases beyond 125 °C, more Cu is incorporated into the Cu_5Sn_6 lattice, and $Cu_{41}Sn_{11}$ begins to nucleate by 175 °C. As the temperature is raised further, more Cu is incorporated, and $Cu_{41}Sn_{11}$ becomes a pure phase.

A very similar reaction occurs in the Co−Sn system, as Co_3Sn_2 is stabilized at a lower temperature, while CoSn can be stabilized at a higher temperature. Figure 4 shows temperature-dependent XRD data for the Co−Sn system, along with simulated XRD data for Co_3Sn_2 and CoSn. As in the Cu−Sn system, the formation of Co_3Sn_2 vs CoSn can be controlled by temperature when the same ratio of reactants is used (1:4 for the Co−Sn system). At 190 °C, the solution with a nominal stoichiometry of Co_1Sn_4 forms a crystalline product that matches that of Co_3Sn_2. The peaks are broad, but the most intense peaks of Co_3Sn_2 match those observed for the sample heated to 190 °C. Furthermore, the SAED pattern for Co_1Sn_4 heated to 190 °C (Figure 5a) matches that expected for Ni_3Sn_2-type Co_3Sn_2, indicating that Co_3Sn_2 is indeed the crystalline phase, and the peak broadening in the XRD data is due to nanocrystalline domains. (This is confirmed by TEM micrographs of the particles, which will be discussed later.) Upon further heating of the nominal Co_1Sn_4 sample, the nanocrystalline Co_3Sn_2 phase converts to CoSn. The XRD pattern for nanocrystalline CoSn matches the simulated data, and the SAED pattern is also consistent with the formation of CoSn (Figure 5b). These data clearly support the idea that the formation of two distinct crystalline phases in the same system can be controlled entirely by

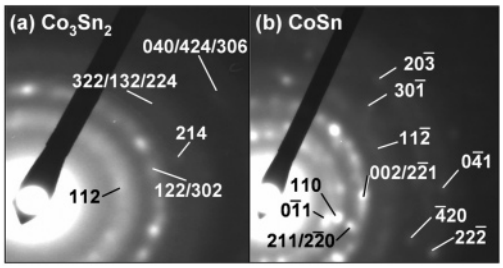

Figure 5. Selected-area electron diffraction patterns for nanocrystalline (a) Co_3Sn_2 and (b) CoSn.

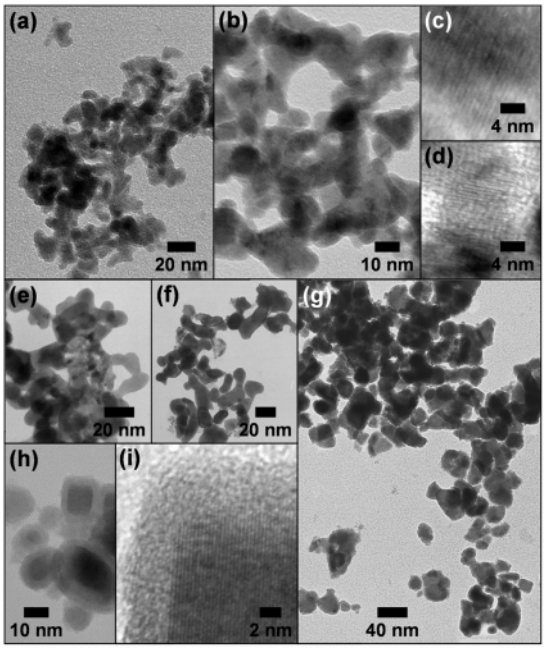

Figure 6. TEM micrographs for nanocrystalline (a) Co_3Sn_2, (b) CoSn, (c) Co_3Sn_2 (high resolution), (d) CoSn (high resolution), (e) PtPb, (f) PtBi, (g) $FeSn_2$ synthesized at 130 °C, and (h,i) Fe_1Sn_6 synthesized at 125 °C, showing the presence of a tin oxide shell surrounding a crystalline $FeSn_2$ core that shows lattice fringes.

temperature and that this reactivity is facilitated by the nanocrystalline phases and the low-temperature solution environment. Such rapid low-temperature reactivity is unprecedented for bulk solid-state systems.

Morphology of Nanocrystalline Intermetallics. While the low-temperature solution route has allowed us to access a variety of binary intermetallic compounds by exploiting the reaction conditions, we have not focused specifically on controlling the morphology of the intermetallic products, although there is precedent for doing so with this synthetic method.[11,23−26] We have found, however, that the as-synthesized products do exhibit interesting nanocrystalline morphologies. TEM micrographs for Co_3Sn_2, CoSn, $FeSn_2$, PtPb, and PtBi are shown in Figure 6. Both Co_3Sn_2 (200 °C) and CoSn (265 °C) appear to be highly irregular networks of fused particles. Lattice fringes (insets to Figures 6a and 6b) highlight the crystalline nature of the nanoparticles, but clearly show polycrystallinity with small domains. By observation of many TEM micrographs (without using statistical analysis), particle sizes appear to range from 5 to 20 nm, while the crystalline domains appear to range in size from 3 to 15 nm. This is qualitatively consistent with the broad peaks in the XRD data presented in Figure 4. PtPb

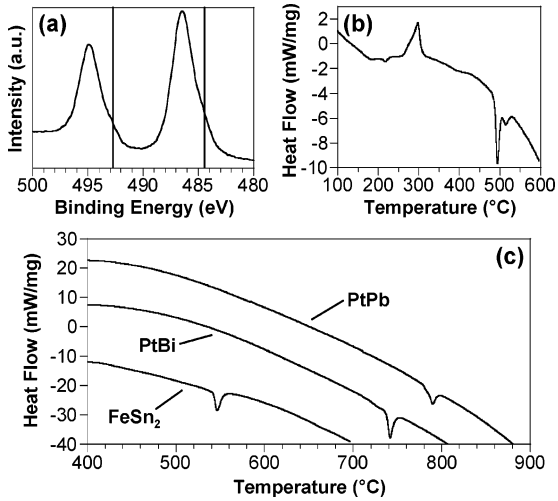

Figure 7. (a) XPS data for the Sn 3d peaks for $FeSn_2$ (vertical lines show the Sn $3d_{3/2}$ and $3d_{5/2}$ peaks for Sn^0); (b) DSC trace from a 1:6 Fe:Sn reaction quenched immediately when the temperature reached 125 °C, prior to complete crystallization of $FeSn_2$ (see text for interpretation of endotherms and exotherms; in the plot, exothermic is up); (c) DSC trace for $FeSn_2$ (phase pure, synthesized at 130 °C), PtPb, and PtBi.

powders synthesized at 165 °C consist of a mixture of spherical and irregular rodlike shapes with average particle sizes that range from approximately 10−30 nm with resolvable lattice fringes. PtBi powders show much larger particles, most likely due to the higher temperature required to nucleate the intermetallic phase (240 °C).

$FeSn_2$ yields larger particles, with diameters that can exceed 50 nm. The $FeSn_2$ powders are highly irregular, much like those of the Co−Sn system. However, many of the $FeSn_2$ particles appear to have a core−shell structure. Because of the large excess of Sn required to yield the $FeSn_2$ intermetallic, our initial hypothesis was that the shell might be SnO_2. XPS was used to characterize the surface of the powder (Figure 7a). The Sn 3d peaks are clearly shifted away from standard Sn^0 values (marked by vertical lines). The higher binding energies indicate the presence of oxidized Sn. Either Sn^{2+} or Sn^{4+} could be present since they are generally indistinguishable because of the large peak width and the small difference in binding energy between the two oxidation states.[38] Regardless, this provides good evidence that the shell is comprised of some SnO_x species. This phenomenon appears in the Co−Sn system as well, as Co_3Sn_2 annealed at 500 °C under Ar shows crystalline SnO_2 by XRD. This is consistent with the SAED pattern for Co_3Sn_2, which shows a wide, diffuse band that matches the most intense peaks for an amorphous tin oxide phase.

The DSC trace (Figure 7b) from a 1:6 Fe:Sn reaction (purposely carried out with excess Sn) that was quenched immediately when the temperature reached 125 °C (e.g., prior to complete crystallization of $FeSn_2$) shows several thermal events. A broad exotherm can be seen with peaks at 280 and 290 °C. A sample heated to 285 °C under flowing Ar revealed a mixture of SnO and $FeSn_2$ by XRD, suggesting that the SnO_x shell is SnO rather than SnO_2. The higher temperature endotherms most likely correspond to decom-

(38) Themlin, J.-M.; Chtaïb, M.; Henrard, L.; Lambin, P.; Darville, J.; Gilles, J.-M. *Phys. Rev. B* **1992**, *46*, 2460−2466.

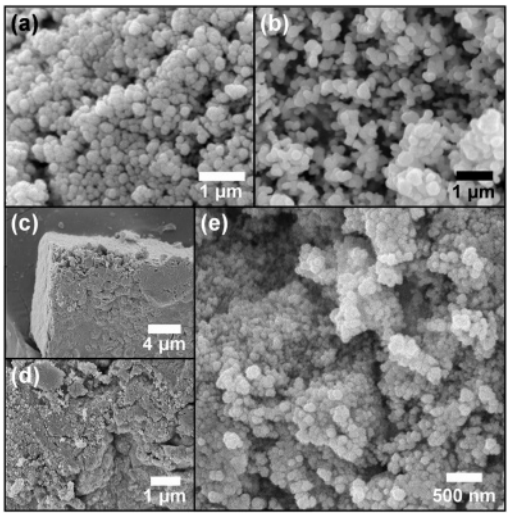

Figure 8. SEM micrographs of (a) PtBi, (b) $FeSn_2$, and (c,d,e) CoSn (three magnifications) nanocrystalline intermetallic powders.

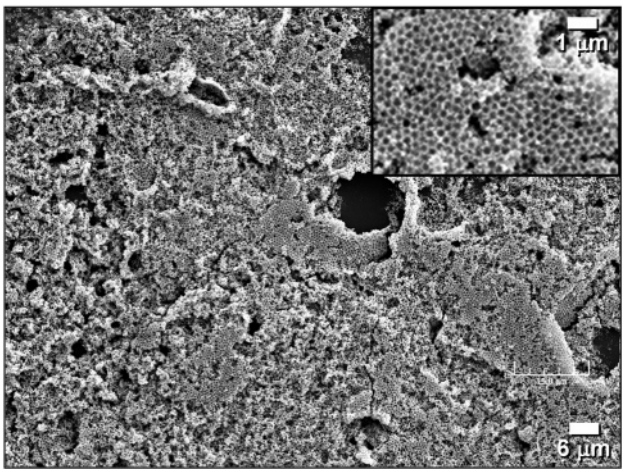

Figure 9. SEM micrograph of intermetallic $FeSn_2$ colloidal crystal replica synthesized by templating against a colloidal crystal of monodisperse 600 nm polystyrene spheres.

position of $FeSn_2$ and SnO_x.[32] Additional DSC studies of intermetallic $FeSn_2$ (phase-pure and crystalline, synthesized at 130 °C), PtPb, and PtBi, shown in Figure 7c, show disordering or decomposition endotherms at temperatures near or slightly lower than their bulk values, as determined from their respective phase diagrams.[32]

Intermetallic powders obtained through traditional solid-state synthesis methods yield micrometer-sized (or larger) particles due to the sintering that is inherent at high temperatures. Figure 8 shows representative SEM images of PtBi, $FeSn_2$, and CoSn powders synthesized using the polyol process. The nanocrystalline powders form spherical aggregates with diameters of 100−150 nm, and these aggregates tend to form densely packed monoliths. In all cases, the intermetallics formed through the polyol process form dense nanocrystalline powders that are difficult to obtain using traditional high-temperature methods.

Solution Processing of Nanocrystalline Intermetallics. It is well-known that metal nanocrystals and nanocrystalline powders synthesized using solution routes offer advantages over traditionally synthesized bulk powders in terms of solution-based materials processing capabilities. For example, polyol-derived metal nanocrystals can be used to form thin films and patterned nanostructures on a variety of substrates,[12,39] and a variety of templated nanomaterials, including nanotubes,[40] inverse opals,[13,41] and hollow nanoscale capsules,[42] can be accessed using standard solution techniques. Because of the difficulty in obtaining solution-dispersible nanocrystalline intermetallic compounds, similar solution-processed intermetallic nanomaterials have remained rare. In Figure 9, we show that intermetallic $FeSn_2$ nanocrystals can be infiltrated into a polystyrene colloidal crystal and converted into a highly porous $FeSn_2$ inverse opal by dissolving the polymer template in toluene. Similar results can be obtained using other nanocrystalline intermetallics as precursors. Preliminary evidence also suggests that nanocrystalline intermetallic thin films are accessible using simple drop coating methods.

Conclusions

In this paper, we demonstrated that the polyol process can be used to synthesize nanocrystalline powders of many late transition-metal and post-transition-metal intermetallic compounds. In some cases, multiple crystalline products can be accessed during the progression of a single reaction, suggesting unusually facile low-temperature solution-mediated reactivity of the nanocrystalline intermetallics. The polyol-derived intermetallics form nanoscale crystallites that range in size from 5 to 100 nm, depending on the system and synthetic conditions, and are amenable to solution-processing capabilities, such as colloidal crystal templating.

The successful synthesis of a large library of nanocrystalline intermetallics using the polyol process has several important implications. First, since the polyol process is known to yield exquisite control over nanocrystal shape and size,[11,23−26] it is reasonable to anticipate that future synthetic modifications will yield similar results. Such an accomplishment would provide access to a wide range of nanomaterials for advanced technological applications and would also facilitate careful size-dependent studies of many important physical phenomena. Second, intermetallic nanoparticles synthesized through this or related methods could prove useful for studies of catalysis and structure−activity relationships on high surface area intermetallic surfaces, providing that the surface chemistry can be appropriately modified and controlled. Third, many emerging applications will increasingly rely on nanocrystalline intermetallics for improved properties, e.g., ductility, hydrogen storage capacity, and thermoelectric efficiency,[43] and the synthetic route described in this work may provide a facile approach for accessing such nanomaterials. Fourth, solution-based routes are common for accessing nanocrystal-derived thin films and templated nanomaterials,[13,39−42] and these nanocrystalline ma-

(39) Guo, Q.; Teng, X.; Yang, H. *Adv. Mater.* **2004**, *16*, 1337−1341.
(40) Sehayek, T.; Lahav, M.; Popovitz-Biro, R.; Vaskevich, A.; Rubinstein, I. *Chem. Mater.* **2005**, *17*, 3743−3748.
(41) Jiang, P.; Bertone, J. F.; Colvin, V. L. *Science* **2001**, *291*, 453−457.
(42) Caruso, F. *Chem. Eur. J.* **2000**, *6*, 413−419.
(43) (a) Birringer, R. *Mater. Sci. Eng. A* **1989**, *117*, 33−43. (b) Gleiter, H. *Prog. Mater. Sci.* **1989**, *33*, 223−315.

terials could significantly expand the availability of intermetallic precursors for such applications. Finally, it is known that the polyol process can yield new and metastable structures not accessible using traditional methods.[10,44] The work described here defines a wide range of intermetallic systems that are accessible using solution methods and opens the door to the discovery of new materials in these and related systems.

(44) (a) Dinega, D. P.; Bawendi, M. G. *Angew. Chem., Int. Ed. Engl.* **1999**, *38*, 1788−1791. (b) Zhao, Y.; Zhang, Y.; Zhu, H.; Hadjipanayis, G. C.; Xiao, J. Q. *J. Am. Chem. Soc.* **2004**, *126*, 6874−6875.

Acknowledgment. This work was supported by start-up funds from Texas A&M University and funding from the Robert A. Welch Foundation (Grant No. A-1583). Acknowledgment is also made to the donors of the Petroleum Research Fund, administered by the American Chemical Society, for partial support of this work. Electron microscopy was performed at the Microscopy and Imaging Center at Texas A&M University. XPS data were acquired at the TAMU/CIMS Materials Characterization Facility. The authors thank William Lackowski for help obtaining and analyzing the XPS data.

CM0520113